Return to Earth: A New Mathematical Model of the Earth's Climate

Stephen Paul Rathbone Wilde, Philip Mulholland[*]

Mulholland Geoscience, Weybridge, Surrey, UK

Email address:
philip.mulholland@uclmail.net (P. Mulholland)
[*]Corresponding author

Abstract: In this paper we use the inverse modelling technique, first applied to the atmosphere of the planet Venus, to demonstrate that the process of convective atmospheric mass motion can be invoked to explain the greenhouse effect of the Earth's climate. We propose that the atmospheric cell is the fundamental element of climate, and have developed an alternative climate model based on this process of atmospheric circulation for a hypothetical tidally locked world. The concept of climate derives from studies by the Greek philosopher Aristotle, who identified the three main climatic zones known to the ancient world; the equatorial torrid zone, the polar frigid zone and in between the favoured temperate zone of the Mediterranean world. Aristotle's three climatic zones can be directly linked to the three main atmospheric circulation cells that we now recognise within the Earth's atmosphere. These three cells are the Hadley cell, the Polar cell and the Ferrel cell. Based on the clear association between the traditional Greek concept of climate and the modern meteorological concept of atmospheric circulation cells, we propose that climate be defined as the presence and action of a particular circulation cell type within a given planetary latitudinal zone. We discuss how with knowledge of three simple meteorological parameters of tropopause elevation, tropopause temperature and lapse rate for each atmospheric cell, combined with the measurement of the area of that cell, the average global surface temperature can be calculated. By means of a mathematical model, the Dynamic-Atmosphere Energy-Transport (DAET) climate model we apply an individual climate analysis to each of the three atmospheric cells, and next generate a parallel composite model of the Earth's planetary climate using these data. We apply the concepts and techniques of the adiabatic version of the DAET climate model, and show how this model can be compared with the published NASA image of the Earth's outgoing long-wave radiation recorded by the CERES (Clouds and the Earth's Radiant Energy System) Instrument onboard the NASA Aqua Satellite. Our analysis of the CERES image suggests that the Tibetan plateau forms a permanent geological thermal radiant leak point in the Earth's atmosphere. We also compare the observed temperature found at the maximum elevation of the Antarctic ice cap with the freezing point of super-cooled water, and suggest that there is therefore a temperature controlled and latent heat related upper limit to the vertical development of a continental icecap.

Keywords: Atmospheric Cell, Climatology, CERES, Climate Model

1. Introduction

The history of Climatology is long and honourable, indeed the very concept of climate goes back to the Greek philosopher Aristotle, who identified the three main types of climatic zone known to the ancient world [1]. These zones are:

A. The Torrid Zone - located to the south of Greece in Africa.

B. The Frigid Zone – located to the far north of Greece where Boreas, the god of the north wind and winter lived.

C. The Temperate Zone of Europe, where the four annual seasons occur, and Greece is most favourably located.

Aristotle's three climatic zones can be directly linked to the three main atmospheric circulation cells that we now recognise within the Earth's atmosphere. These three cells are:

A. The Hadley cell [2], which is a thermal cell, driven by solar radiation from space heating the planet's surface. Two zones of Hadley cells exist in our atmosphere, these are both found in the Tropics and are generally located between the Equator and the Tropic of Cancer in the northern hemisphere and the Tropic of Capricorn in

the south. The Hadley cell's poleward limit is located in the Horse Latitudes; where a zone of descending air exists forming surface high pressure anticyclones. It is the Hadley cell that is the defining atmospheric feature of Aristotle's Torrid Zone.

B. The Polar cell [3], which is also a thermal cell, but it is driven by atmospheric circulation caused by radiation cooling from the ground surface directly to space. This radiative cooling produces an atmospheric surface inversion, that is most noticeable in winter. The Polar cell's equatorward limit is marked by the Polar Front, an oscillating band with an associated strong horizontal surface temperature gradient; above which is found the jet stream of the upper troposphere. The Polar cell is responsible for the formation and surface export towards the equator of cold dense airmasses. It is the Polar cell that is the defining atmospheric feature of Aristotle's Frigid Zone.

C. The Ferrel cell [4], which is a mechanical cell, located between the Hadley and Polar cells. It acts as a buffer or cog between the latitudinal limits of the two thermal cells, and has a circulation pattern that abuts and links these two opposing cells. The Ferrel cell forms a zone of mixing and ascending air that is associated with cold cored cyclones. It is the Northern Hemisphere Ferrel cell that accounts for Aristotle's Temperate Zone, with its annual seasonal changes and varied weather patterns.

In this paper we adopt the climate modelling techniques first applied to the planet Venus [5] where we developed an alternative climate model, using the process of atmospheric circulation on a hypothetical tidally locked planet. We use this model to demonstrate that convective atmospheric mass motion recycling can be invoked to explain the planetary greenhouse effect. We use here the modelling strategy of Noonworld and by creating a three-element parallel model constrained to atmospheric data, apply this concept of convective atmospheric mass-motion energy recycling to study the climate of the Earth.

In building a three-element parallel model the primary distinction being studied is between slowly rotating Venus, with its hemisphere encompassing pair of Hadley cells, and rapidly rotating Earth, with its triple cell per hemisphere configuration of Hadley, Polar and Ferrel cells [2-4].

The use of a parallel configuration for the model design addresses the issue that the primary motion of the Earth's atmosphere is predominantly zonal and not meridional flow, and that tropospheric air motion is constrained by the Coriolis effect [6]. This design also addresses a feature of tropical climate best summed up as "Nighttime is the winter of the tropics."

The issue of planetary axial tilt, leading to polar winters dominated by little or no solar flux and summers with no nighttime, was addressed by splitting the polar cell sub-unit in the climate model into two distinctly separate modes of operation. For the summer all convective activity is assumed to recycle the descending air directly back onto a lit arctic surface. By this means the low intensity solar flux inherent at high latitudes is amplified by a process of atmospheric short-circuiting during the arctic summer. By contrast during the arctic winter the polar sub-cell unit in the model is assumed to have zero solar influx, and all of the power intensity used to drive the atmospheric circulation arrives by advection from the adjacent Ferrel cell.

Finally, we have adopted in the model a nuanced approach to the issue of lapse rate, using a wet adiabatic lapse rate for the Hadley cell, an intermediate environmental lapse rate for the Ferrel cell, and a dry adiabatic lapse rate for the Polar cell. This approach is in contrast to previous work into the study of terrestrial radiation, where a uniform planetary lapse rate of 6°C/km was used across all atmospheric cells [7].

2. Methodology

Our modern understanding of the dynamics of the Earth's planetary climate, and the role that radiant energy has in defining the features of the atmospheric circulation system, has progressed with the formulation of the energy budget diagram used to quantify and rank the importance of the constituent elements of the climate system [8]. A key metric of the energy budget is the standard Vacuum Planet or rapidly rotating airless planet equation [9]. This equation is used in Climate Science to calculate the expected thermal emission temperature T_e of an illuminated globe under the average solar irradiance that pertains for a planet's average orbital distance from the sun, and for that planet's specific Bond albedo.

"The equilibrium temperature T_e of an airless, rapidly rotating planet is:

Equation 1: $T_e \equiv [S \pi R^2 (1-A)/4 \pi R^2 \varepsilon \sigma]^{1/4}$

where σ is the Stefan-Boltzmann Constant, ε the effective surface emissivity, A the wavelength-integrated Bond albedo, R the planet's radius (in metres), and S the solar constant (in Watts/m^2) at the planet's average distance from the sun."

The results of applying this Vacuum Planet equation to the Earth are shown in Table 1:

Table 1. *The Expected Surface Temperature for an Airless Earth compared with its actual Atmospheric Temperature.*

Parameter	Symbol	Earth	Units	Dimensions
Solar Constant at distance a	S	1361	W/m^2	MT^{-3}
Radius of Body	R	6,367,445	m	L
Bond Albedo	A	0.306	Constant	Constant A
Stefan-Boltzmann Constant	σ	5.67E-08	W/m^2/K^4	MT^{-3}K^{-4}
Effective surface emissivity	ε	1	Constant	Constant ε
Expected Te	T_e	254	Kelvin	K
Greenhouse Effect	GE	34	Kelvin	K
Actual Ts	T_s	288	Kelvin	K
Distance from the Sun	a	1.4960E+11	m	L

2.1. Applying the Dynamic-Atmosphere Energy-Transport (DAET) Model to the Study of Earth's Climate

We are attempting here to simultaneously analyse the energy flows for the Earth's three atmospheric circulation cells, using the adiabatic form of the Dynamic-Atmosphere Energy-Transport (DAET) model, previously used for the study of the climates of Venus and Titan [5, 10]. The Earth is

modelled as a spherical globe that cuts a circular silhouette, or disk shadow from the beam of the solar irradiance at the planet's average orbital distance from the Sun. The average fraction of the illumination beam, that the silhouette for each of the three circulation cells intercepts during the course of a year, is latitude dependent.

For the purpose of this analysis it is assumed that the latitudinal reach of the Hadley cell for each hemisphere is from the equator to latitude 30°. The Ferrel cell extends from latitude 30° to the (ant) arctic circle and the Polar cell occupies the remaining latitudes around the pole of rotation. The tropical Hadley cell of net energy surplus intercepts 60.90% of the illumination, the temperate mechanical Ferrel cell of energy transport intercepts 36.29%, and the frigid thermal Polar cell of net energy deficit intercepts the remaining 2.81% of the Sun's energy cut out by the disk silhouette (Figure 1).
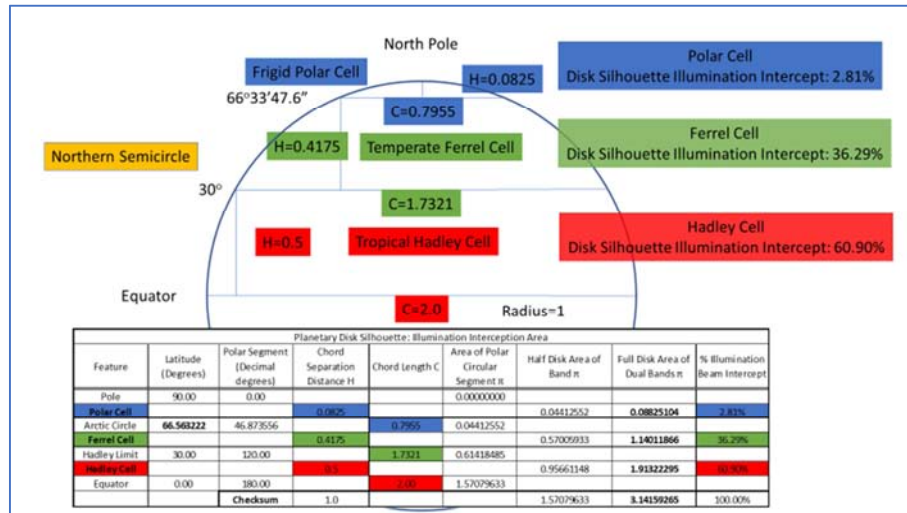

Figure 1. Earth's Planetary Disk Silhouette for the average annual axial tilt of the globe.

The Earth has the form of a globe, and because of this spherical shape the surface of the Earth is unevenly illuminated. The location of the maximum possible power intensity at the surface of the Earth occurs at the solar zenith, the unique point on the Earth's surface where the Sun is directly overhead. At all other locations the slant of the Earth's surface to the sun's beam of light lowers the interception intensity. This is a feature of illumination that we observe at both dawn and dusk when our shadows reach their maximum length as the sunlight grazes the surface of the Earth.

The average power intensity at the Earth's surface is different for each of the three atmospheric cells. The tropical Hadley cells, which occupy 50% of the surface of the Earth, intercept 60.90% of the beam silhouette, and therefore receive the highest radiant beam intensity. The Ferrel cells, which occupy 36.29% of the surface of the Earth, intercept 41.75% of the beam silhouette and therefore receive a lower radiant beam intensity; while the Polar cells, which occupy 8.25% of the surface of the Earth, intercept only 2.81% of the disk silhouette, and therefore receive the lowest average radiant beam power intensity. This quantity of radiant power intensity is defined by the illumination power intensity dilution divisor or "divide by rule" that is specific for each of the three atmospheric cells. This metric is used to constrain the value of the insolation flux used in the modelling process (Figure 2).
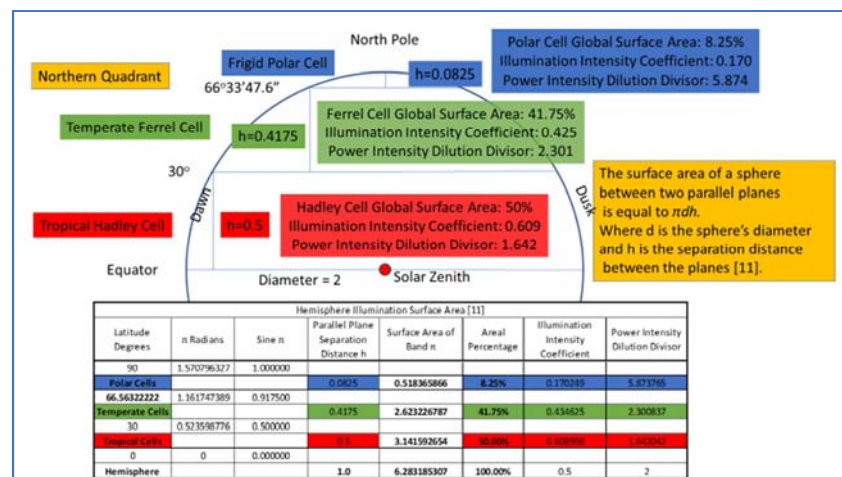

Figure 2. Globular Earth's Lit Hemisphere Illumination Intensity for the average annual surface attitude of the planet [11].

The power intensity of the Earth's average annual irradiance is 1361 W/m² [12]. This flux which arrives at the Top of the Atmosphere (TOA) is then reduced by the Earth's planetary Bond albedo of 0.306 that acts as a bypass filter diverting radiant solar energy back out to space [12]. It is only the remaining 69.4% of the radiant flux which is absorbed by the planet, and consequently the value of the solar irradiance that drives the Earth's climate is reduced to a power intensity of 944.53 W/m² (Figure 3).

It is fundamental to what comes next that the following aspect of power intensity distribution within the Earth's climate system is appreciated in its full subtlety and implications. In figure 1 we observed that the planet intercepts sunlight as if it is a planar disk. However, because of the attitude (slant) of the surface of a sphere with respect to the parallel rays within the solar beam, the strength of the beam striking the surface decreases from its maximum possible post-albedo value of 944.53 W/m² at the solar zenith, down to a value of zero at the terminator, the great circle line of dawn and dusk (Figure 3).
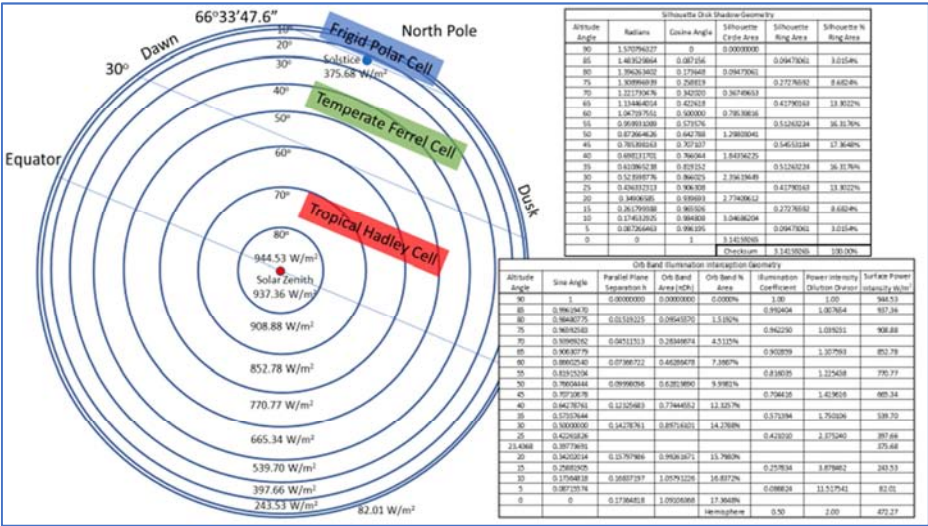

Figure 3. *The Scaled Model Globular Earth's Lit Hemisphere Illumination Interception Geometry.*

Perhaps the most fundamental issue at the heart of climate modelling is the use of the power intensity illumination divisor of integer 4, that is present in the vacuum planet equation (Equation 1). In this special case divisor 4 is used to dilute the insolation to one quarter of the radiant beam intensity. The original, valid and only purpose of the vacuum planet equation is to establish the radiant *exhaust* temperature of an illuminated planetary body. Planetary bodies of whatever shape or form are only ever illuminated over the surface of a single hemisphere. So, the appropriate divisor required to calculate the average insolation power intensity for the climate system, supplied by the fully lit face of a planet, is integer 2.

Furthermore, there will exist on every lit planet a unique location, the solar zenith, at which the radiant power intensity at the base of the atmosphere is exactly equal to the value of the solar irradiance at that planet's orbital distance from the sun (Figure 3). It should again be appreciated that the power intensity illuminating the planet's atmosphere at the solar zenith is scaled down by the Bond albedo which acts as a bypass filter. The albedo filter acts by removing insolation from the climate system, and returning this discarded portion of the high-frequency radiant flux directly back to space.

2.2. Calculating the Average Surface Temperature of the Earth

The Earth's atmosphere is a dynamic system composed of three zonally separated and interlocking cells that are symmetrically distributed in each hemisphere (Figure 1). The global areal distribution of each atmospheric cell is shown in Figure 2. The higher percentage of insolation intercepted by the tropical Hadley cells, compared to the low value intercepted by the Polar cells, means that less surface power intensity is delivered to the boreal regions of the planet (Figure 3). The weakened strength of the sunlight in the arctic, caused by the sun's lower angle of elevation in the sky, is a fundamental reason for the lower average surface temperatures found at the poles.

For each atmospheric cell we can compute the average surface temperature if we know the average annual values of the following meteorological parameters:

1. The average height of the tropopause.
2. The average temperature of the tropopause.
3. The average environmental lapse rate of each cell.

Using these three metrics we can then calculate the average surface temperature of each atmospheric circulation cell (Table 2).

Table 2. *Atmospheric Cell Parameters.*

Cells	Hadley	Ferrel	Polar
Tropopause Height (km)	17	13	9
Tropopause Temperature (Celsius)	-83	-78	-78.5
Environmental Lapse Rate (K/km)	6.5	6.5	6.5
Average Annual Surface Temperature (Celsius)	27.9	6.5	-20.0

From our knowledge of the average surface temperature for each atmospheric cell (Table 2) combined with our calculation of the global areal footprint for each cell (Figure 2) we can now calculate the global average surface temperature of the Earth. The key parameters are the global extent of each of the three meteorological cells of Hadley, Ferrel and Polar, and their respective average annual temperatures. By combining these three temperature values and using an area weighted average, the average annual temperature of the whole planet can be derived (Table 3).

Table 3. Calculating the Global Average Temperature of the Earth.

Cell Type	Hadley	Ferrel	Polar
Percentage of Global Area	50.00%	41.75%	8.25%
Cell Average Temperature (Celsius)	27.9	6.5	-20.0
Area Weighted Proportion AW% (Celsius)	13.94	2.71	-1.65
Average Annual Global Temperature (Celsius) AW% of Hadley+AW% of Ferrel+AW% of Polar	15.0		

2.3. Applying the Dynamic-Atmosphere Energy-Transport (DAET) Climate Model to the Earth

The Dynamic-Atmosphere Energy-Transport (DAET) climate model contains a mechanism for energy flux recycling using the meteorological process of atmospheric circulation. This model was used to demonstrate that convective atmospheric mass motion can be invoked to explain the planetary greenhouse effect for both Venus and also Titan, the tidally locked moon of Saturn [5, 10]. Atmospheric data for these two bodies show that there is little or no thermal contrast between the lit daytime and the dark nighttime hemispheres on these slowly rotating worlds. Our studies indicate that when applied to slowly rotating Venus, or the moon Titan, the adiabatic model required only a single energy flux partition ratio, common to both the lit and dark sides of each globe, to achieve an appropriate thermal boost within these atmospheres.

However, when a single common energy partition ratio was applied to the process of creating an adiabatic model for the Hadley cell on rapidly rotating Earth, the model failed and created an atmosphere in which the tropopause is higher on the unlit dark side of the globe (Table 6, Attempt 0). Clearly this result is in direct contrast to observed atmospheric data, where we find that the convective process on the lit hemisphere produces a tropopause with a higher elevation during the hours of daylight compared to the nighttime. The solution to this failure of the analysis is to apply two distinct and separate energy partition ratios during the process of inverse modelling, one for each side. On the lit side of energy collection, the partition ratio should be biased in favour of the air. However, on the dark side of energy loss, the partition ratio should be biased in favour of the radiant surface of energy loss to space.

The justification for using two distinct energy partition ratios, for the atmospheric circulation cells on rapidly rotating Earth, is based on observation and deduction. The primary observation is that for the Earth atmospheric convection is predominantly a sunlight driven phenomenon. It creates turbulent air motion at the lit surface boundary of the planet, and in the presence of a gravity field turbulent mixing favours energy retention by the air over direct surface radiant energy loss to space.

Contrastingly at night, in the absence of solar radiant loading, the process of surface radiant cooling predominates as the atmosphere stabilises and develops a surface inversion of cold dense air. This near surface vertical thermal profile results in lateral movement of dense air downslope, away from land surface high-elevation points of radiantly efficient emission to space. Consequently, at these locations the overlying air preferentially delivers retained and advected daytime acquired thermal energy down onto the now cooler nighttime surface.

The parameters listed in Table 4 have been used to constrain the adiabatic climate modelling process:

Table 4. Earth Climate Metrics used to constrain the three-element parallel cell DAET climate model.

Earth Climate Metrics	
Earth's TOA Solar Irradiance W/m^2	1361.0
Earth Bond Albedo	0.306
Dimmed Intercepted Beam at Solar Zenith W/m^2	944.53
Earth Hemisphere Average Distribution W/m^2	472.27
Disk Silhouette of Tropical Hadley Cell	60.90%
Disk Silhouette of Temperate Ferrel Cell	36.29%
Disk Silhouette of Frigid Polar Cell	2.81%
Global Surface Area of Tropical Hadley Cell	50.00%
Global Surface Area of Temperate Ferrel Cell	41.75%
Global Surface Area of Frigid Polar Cell	8.25%
Hadley Cell Power Intensity Dilution Divisor	1.642042
Ferrel Cell Power Intensity Dilution Divisor	2.300839
Polar Cell Power Intensity Dilution Divisor	5.873730
Average Daily Hadley Cell Illumination W/m^2	575.22
Average Daily Ferrel Cell Illumination W/m^2	410.52
Average Daily Polar Cell Illumination W/m^2	160.81
Hadley Annual Surface Temperature (Celsius)	27.9
Ferrel Annual Surface Temperature (Celsius)	6.5
Annual Polar Surface Temperature (Celsius)	-20.0
Tropical Wet Lapse Rate (K/km)	4.6
Temperate Lapse Rate (K/km)	6.5
Frigid Dry Lapse Rate (K/km)	8.8

2.3.1. Modelling the Earth's Hadley Cell

The two planetary Hadley cells, present in the tropics of the northern and southern hemispheres, together occupy 50% of the surface area of the Earth (Table 4), and in total intercept 60.90% of the light that creates the disk silhouette of the planetary beam shadow (Table 4). Because the surface area of the globe's lit hemisphere is twice the cross-sectional area of the total disk silhouette, it follows that the power intensity illumination divisor for the Hadley cells has a value of (0.5*2)/0.609=1.642 (Table 4). This divisor is then applied to the post-albedo dimmed irradiance to create the Hadley cell specific power intensity flux of 575.22 W/m^2. This flux is then in turn used to analyse the process of energy recycling within the Earth's Hadley cell by atmospheric mass motion using the adiabatic climate model of the captured solar energy (Table 5).

Table 5. The inverse modelling process used to determine the dual power intensity flux partition ratios for the Earth's Hadley cell.

Cycle Number	Hadley Incoming Captured Radiation	Heating the Hadley Cell Lit side	Lit side Hadley Cell Radiant Loss to Space	Lit side Hadley Cell Thermal Export to Dark Side	Darkside Hadley Cell Radiant Loss to Space	Darkside Hadley Cell Thermal Return to Litside	Radiant Energy Exiting Tropical Zone to Space
	Hadley Partition Ratio: Target Annual Temperature 300.9 Kelvin (27.9oC)		24.1541%	75.8459%	53.8273%	46.1727%	
0	575.22					0	
1	575.2191101	575.2191101	138.9391858	436.2799243	234.8378307	201.4420936	373.7770165
2	575.2191101	776.6612037	187.5957759	589.0654278	317.0781865	271.9872413	504.6739624
3	575.2191101	847.2063514	204.6353443	642.5710071	345.8788108	296.6921963	550.5141551
4	575.2191101	871.9113065	210.6026119	661.3086946	355.9648075	305.3438871	566.5674194
696	575.2191101	885.2257096	213.8185904	671.4071191	361.4005197	310.0065994	575.219110121
697	575.2191101	885.2257096	213.8185904	671.4071191	361.4005197	310.0065994	575.219110121
698	575.2191101	885.2257096	213.8185904	671.4071191	361.4005197	310.0065994	575.219110121
699	575.2191101	885.2257096	213.8185904	671.4071191	361.4005197	310.0065994	575.219110121
700	575.2191101	885.2257096	213.8185904	671.4071191	361.4005197	310.0065994	575.219110121
Cycle Number	Proportionate Hadley Insolation	Heating the Hadley Cell Litside	Lit side Hadley Cell Radiant Loss to Space	Lit side Hadley Cell Thermal Export to Dark Side	Darkside Hadley Cell Radiant Loss to Space	Darkside Hadley Cell Thermal Return to Litside	Radiant Energy Exiting Tropical Zone to Space
Infinity	575.22	885.23	213.82	671.41	361.40	310.01	575.22
S-B	5.67E-08	5.67E-08	5.67E-08	5.67E-08	5.67E-08	5.67E-08	5.67E-08
Kelvin	317.4	353.5	247.8	329.9	282.6	271.9	317.4
Celsius	44.4	80.5	-25.2	56.9	9.6	-1.1	44.4
	Statistic	Mean Exit Temp	Mean Air Temp	Lit-side	Dark-side	Hadley Average	
	Kelvin	265.18	300.90	W/m2	W/m2	W/m2	
	Celsius	-7.82	27.9	885.226	671.407	778.316	
	Atmospheric Response		Thermal Enhancement (Kelvin)	Lapse rate K/Km	Tropopause Height (km) Delta K	Km	
	Daytime Hadley Cell		36.1	4.6	82.1	18.0	
	Nighttime Hadley Cell			4.6	47.3	10.4	

The objective of the inverse modelling process used in Table 5 is to establish the daytime convection and nighttime advection pair of energy partition ratios for both of the atmospheric circulation cells. The inverse modelling process is constrained by the two known parameters of annual average temperature and also the average tropopause height for the energy collection (lit side) of each cell. The process of establishing these partition ratios (daytime and nighttime) for the Earth's Hadley cell involved a sequence of tuning that required a "see-saw" approach of iterative "nudges" (Table 6).

Starting with a neutral nighttime energy partition ratio of 50% radiant loss to space and 50% thermal retention by the air, the inverse modelling process was run with the objective of establishing the lit surface energy partition ratio that creates a daytime tropopause height of 18 km (Table 6, Attempt 1). This first attempt resulted in an adiabatic model of the Hadley cell with an average annual temperature of 33.75°C, which is warmer than the required average temperature of 27.9°C.

In order to reduce the model temperature to the required value of 27.9°C the inverse modelling process was then repeated, but this time adjusting the nighttime energy partition ratio to achieve an increased energy loss to space from the dark side, thereby reducing the average temperature to the required value (Table 6, Attempt 2). This second attempt produced a modelling result in which the daytime tropopause height of 17.8 km is too low.

This undershoot was then corrected by repeating the search for the lit side energy partition ratio that creates a tropopause height of 18 km (Table 6, Attempt 3). This third attempt to tune the model by increasing the retention of flux into the air on the lit side produces an average annual temperature of 28.25°C, which is still too warm.

The fourth attempt, with its increased nighttime radiant loss to space, cools the return flow of air to the lit side sufficiently to successfully achieve both targets of a lit hemisphere tropopause height of 18 km, and an average annual temperature of 27.9°C (Table 6, Attempt 4).

Table 6. Establishing the dual set of energy partition ratios for the Earth's Hadley cell.

Adiabatic Nudge	Lit side of Energy Surplus		Dark Side of Energy Deficit		Hadley Average Air Temperature °C	Hadley Average Radiant Temperature °C	Tropopause Height (km)		Comments
Attempt	Loss to Space	Air Retention	Loss to Space	Air Retention			Lit Side	Dark Side	
0	37.7351%	62.2649%	37.7351%	62.2649%	27.90	-7.51	8.2	15.1	Single Ratio Adiabatic Model. Lit side Tropopause is lower than dark side
1	24.3854%	75.6146%	50.0000%	50.0000%	33.75	-7.31	18.0	11.6	Lit side Tropopause Target 18

Adiabatic Nudge Attempt	Lit side of Energy Surplus		Dark Side of Energy Deficit		Hadley Average Air Temperature °C	Hadley Average Radiant Temperature °C	Tropopause Height (km)		Comments
	Loss to Space	Air Retention	Loss to Space	Air Retention			Lit Side	Dark Side	
2	24.3854%	75.6146%	53.6077%	46.3923%	27.90	-7.71	17.8	10.4	km: Hadley is too warm Target 27.9°C: Lit side Tropopause is too low
3	24.1541%	75.8459%	53.6077%	46.3923%	28.25	-7.79	18.0	10.4	Target 18 km: Hadley is too warm
4	24.1541%	75.8459%	53.8273%	46.1727%	27.90	-7.82	18.0	10.4	Both Targets Reached Successfully

2.3.2. Modelling the Earth's Ferrel Cell

The process of establishing the dual component flux partition ratio for the Ferrel cell adopts the same strategy as that established for the Hadley cell described in Section 2.3.1.

The two planetary Ferrel cells, present in the temperate zones of the northern and southern hemispheres, together occupy 41.75% of the surface area of the Earth (Table 4) and in total intercept 36.29% of the light that creates the disk silhouette of the planetary beam shadow (Table 4). Because the surface area of the globe's lit hemisphere is twice the cross-sectional area of the total disk silhouette, it follows that the power intensity illumination divisor for the Ferrel cells has a value of (0.4175*2)/0.3629=2.3008 (Table 4). This divisor is then applied to the post-albedo dimmed irradiance to create the Ferrel cell specific power intensity flux of 410.52 W/m². This flux is then in turn used to analyse the process of recycling of the captured solar energy by atmospheric mass motion, within the Earth's Ferrel cell using the adiabatic climate model (Table 7).

Table 7. The inverse modelling process used to determine the dual power intensity flux partition ratios for the Earth's Ferrel cell.

Cycle Number	Ferrel Incoming Captured Radiation	Heating the Ferrel Cell Lit side	Ferrel Thermal Radiation Loss to Space	Ferrel Cell Export to Dark Side	Darkside Ferrel Cell Radiant Loss to Space	Darkside Ferrel Cell Thermal Return to Litside	Radiant Energy Exiting Temperate Zone to Space
	Ferrel Partition Ratio: Target Annual Temperature 279.5 Kelvin (6.5°C)		21.6206%	78.3794%	54.2258%	45.7742%	
0	410.52					0	
1	410.5171466	410.5171466	88.7562776	321.7608690	174.4772691	147.2835999	263.2335467
2	410.5171466	557.8007465	120.5998782	437.2008683	237.0754834	200.1253849	357.6753616
3	410.5171466	610.6425315	132.0245901	478.6179414	259.5342051	219.0837363	391.5587952
4	410.5171466	629.6008829	136.1234998	493.4773831	267.5918499	225.8855332	403.7153497
696	410.5171466	640.2083996	138.4169087	501.7914909	272.1002379	229.6912530	410.5171466
697	410.5171466	640.2083996	138.4169087	501.7914909	272.1002379	229.6912530	410.5171466
698	410.5171466	640.2083996	138.4169087	501.7914909	272.1002379	229.6912530	410.5171466
699	410.5171466	640.2083996	138.4169087	501.7914909	272.1002379	229.6912530	410.5171466
700	410.5171466	640.2083996	138.4169087	501.7914909	272.1002379	229.6912530	410.5171466
Cycle Number	Proportionate Ferrel Insolation	Boosted Ferrel Temperature	Ferrel Thermal Radiation Loss to Space	Ferrel Cell Export to Dark Side	Darkside Ferrel Cell Radiant Loss to Space	Darkside Ferrel Cell Thermal Return to Litside	Radiant Energy Exiting Temperate Zone to Space
Infinity	410.517	640.208	138.417	501.791	272.100	229.691	410.517
S-B	5.67E-08	5.67E-08	5.67E-08	5.67E-08	5.67E-08	5.67E-08	5.67E-08
Kelvin	291.7	326.0	222.3	306.7	263.2	252.3	291.7
Celsius	18.7	53.0	-50.7	33.7	-9.8	-20.7	18.7
	Statistic	Mean Exit Temp	Mean Air Temp	Lit-side	Dark-side	Ferrel Average	
	Kelvin	242.74	279.50	W/m2	W/m2	W/m2	
	Celsius	-30.26	6.50	640.208	501.791	571.000	
	Atmospheric Response		Thermal Enhancement (Kelvin)	Lapse rate K/Km	Tropopause Height (km) Delta K	Km	
	Daytime Ferrel Cell		34.3	6.5	84.4	13.0	
	Nighttime Ferrel Cell			6.5	43.5	6.7	

As with the Hadley cell model the determination of the parameters for the Ferrel cell starts with a neutral nighttime energy partition ratio of 50% radiant loss to space and 50% thermal retention by the air. The inverse modelling process is then run with the objective of establishing the lit surface energy partition ratio that creates a daytime tropopause height of 13 km, for an average annual cell temperature of 6.5°C. As with the analysis of the Hadley cell, a process of "see-saw" iterations were used to achieve the final pair of partition ratios that satisfy both of these data constraints for the Ferrel cell (Table 8).

Table 8. *Establishing the dual set of energy partition ratios for the Earth's Ferrel cell.*

Adiabatic Nudge	Lit side of Energy Surplus		Dark Side of Energy Deficit		Ferrel Average Air Temperature °C	Ferrel Average Radiant Temperature °C	Tropopause Height (km)		Comments
Attempt	Loss to Space	Air Retention	Loss to Space	Air Retention			Lit Side	Dark Side	
0	36.7784%	63.2216%	36.7784%	63.2216%	6.50	-28.90	5.8	10.1	Single Ratio Adiabatic Model. Lit side Tropopause is lower than dark side
1	21.9039%	78.0961%	50.0000%	50.0000%	12.66	-29.59	13.0	7.6	Lit side Tropopause Target 13 km: Ferrel is too warm
2	21.9039%	78.0961%	53.9690%	46.0310%	6.50	-30.11	12.8	6.7	Target 6.5°C: Lit side Tropopause is too low
3	21.6206%	78.3794%	53.9690%	46.0310%	6.90	-30.22	13.0	6.7	Target 13 km: Ferrel is too warm
4	21.6206%	78.3794%	54.2258%	45.7742%	6.50	-30.26	13.0	6.7	Both Targets Reached Successfully

2.3.3. Modelling the Earth's Polar Cell

The two planetary polar cells together occupy 8.25% of the surface area of the Earth (Table 4) and in total intercept only 2.81% of the light that creates the disk silhouette of the planetary beam shadow (Table 4). As before, because the surface area of the globe's lit hemisphere is twice the cross-sectional area of the total disk silhouette, it follows that the power intensity illumination divisor for the Polar cells has a value of (0.0825*2)/0.0281=5.874 (Table 4). When this divisor is applied to the silhouette of the post-albedo dimmed irradiance it creates the Polar cell specific power intensity flux of 160.81 W/m^2.

Modelling tests established that this power intensity can be used to create an average annual Polar cell temperature of minus 20°C (Table 9).

Table 9. *Testing the model of energy partition ratios for the Earth's Polar cells.*

Adiabatic Nudge	Lit side of Energy Surplus		Dark Side of Energy Deficit		Polar Average Air Temperature °C	Polar Average Radiant Temperature °C	Tropopause Height (km)		Comments
Attempt	Loss to Space	Air Retention	Loss to Space	Air Retention			Lit Side	Dark Side	
0	25.5567%	74.4433%	25.5567%	74.4433%	-20.00	-79.34	7.0	8.6	Single Ratio Adiabatic Model. Lit side Tropopause is lower than dark side
1	17.9095%	82.0905%	50.0000%	50.0000%	-42.26	-81.94	9.0	4.5	Lit side Tropopause Target 9 km: Polar is too cold
2	17.9095%	82.0905%	34.5138%	65.4862%	-20.00	-79.89	9.6	7.1	Target -20°C: Lit side Tropopause is too high
3	19.3021%	80.6979%	34.5138%	65.4862%	-22.31	-79.55	9.0	7.0	Lit side Tropopause Target 9 km: Polar is too cold
4	19.3021%	80.6979%	33.0183%	66.9817%	-20.00	-79.42	9.1	7.3	Target -20°C: Lit side Tropopause is too high
5	19.4497%	80.5503%	33.0183%	66.9817%	-20.25	-79.39	9.0	7.3	Lit side Tropopause Target 9 km: Polar is too cold
6	19.4497%	80.5503%	32.8566%	67.1434%	-20.00	-79.37	9.0	7.3	Both Targets Reached Successfully

The stable value that results from this initial test, and presented in Table 10 achieves an average annual temperature of minus 20°C for the Polar cell. However, the range of minimum average air temperature from minus 7.4°C for the summer to minus 32.6°C for the winter is actually too small to account for the known winter extrema air temperatures observed in polar regions. For example, air temperatures of lower than minus 50°C for July were recorded during advected katabatic drainage storms at the Little America exploration base, on the ice edge of the Ross Sea in Antarctica [13].

Table 10. *The inverse modelling process used to test the interlocked dual power intensity flux partition ratios for the Earth's Polar cells.*

Cycle Number	Polar Incoming Captured Radiation	Heating the Polar Cell Lit side	Lit side Polar Cell Radiant Loss to Space	Lit side Polar Cell Thermal Export to Dark Side	Dark side Polar Cell Radiant Loss to Space	Dark side Polar Cell Thermal Return to Lit side	Radiant Energy Exiting Polar Zone to Space
	Polar Partition Ratio: Target Annual Temperature 253 Kelvin (-20°C)		19.4497%	80.5503%	32.8566%	67.1434%	
0	160.81					0	
1	160.8064999	160.8064999	31.27644873	129.5300512	42.55911054	86.97094068	73.83555927
2	160.8064999	247.7774406	48.19207196	199.5853687	65.57687337	134.0084953	113.7689453
3	160.8064999	294.8149952	57.34075479	237.4742404	78.02585079	159.4483896	135.3666056
4	160.8064999	320.2548896	62.28874851	257.9661411	84.75878308	173.2073580	147.0475316
696	160.8064999	350.2205534	68.11699269	282.1035607	92.68950726	189.4140534	160.8064999

Cycle Number	Polar Incoming Captured Radiation	Heating the Polar Cell Lit side	Lit side Polar Cell Radiant Loss to Space	Lit side Polar Cell Thermal Export to Dark Side	Dark side Polar Cell Radiant Loss to Space	Dark side Polar Cell Thermal Return to Lit side	Radiant Energy Exiting Polar Zone to Space
697	160.8064999	350.2205534	68.11699269	282.1035607	92.68950726	189.4140534	160.8064999
698	160.8064999	350.2205534	68.11699269	282.1035607	92.68950726	189.4140534	160.8064999
699	160.8064999	350.2205534	68.11699269	282.1035607	92.68950726	189.4140534	160.8064999
700	160.8064999	350.2205534	68.11699269	282.1035607	92.68950726	189.4140534	160.8064999
Cycle Number	Proportionate Polar Insolation	Heating the Polar Cell Lit side	Lit side Polar Cell Radiant Loss to Space	Lit side Polar Cell Thermal Export to Dark Side	Dark side Polar Cell Radiant Loss to Space	Dark side Polar Cell Thermal Return to Lit side	Radiant Energy Exiting Polar Zone to Space
Infinity	160.81	350.22	68.12	282.10	92.69	189.41	160.81
S-B	5.67E-08	5.67E-08	5.67E-08	5.67E-08	5.67E-08	5.67E-08	5.67E-08
Kelvin	230.8	280.3	186.2	265.6	201.1	240.4	230.8
Celsius	-42.2	7.3	-86.8	-7.4	-71.9	-32.6	-42.2

Statistic	Mean Exit Temp	Mean Air Temp	Lit side	Dark side	Polar Average
Kelvin	193.63	253.0	W/m2	W/m2	W/m2
Celsius	-79.37	-20.0	350.221	282.104	316.162

Atmospheric Response	Thermal Enhancement (Kelvin)	Lapse rate K/Km	Delta K	Tropopause Height (km) Km
Daytime Polar Cell	49.6	8.8	79.4	9.0
Night time Polar Cell		8.8	64.5	7.3

Modern icecap temperature data recorded for Antarctica regularly reach values of minus 70°C in winter (Figure 4), and so an alternative modelling strategy was devised to account for these extreme temperature values recorded for winter in polar regions.
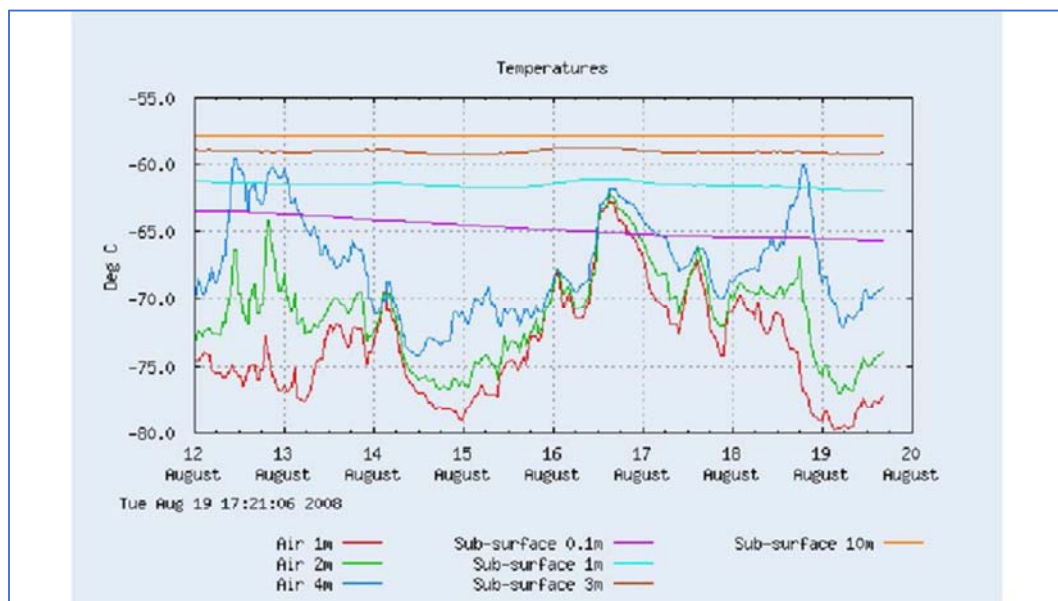

Figure 4. *Australian Antarctic Division [14]: Dome Argus Temperature Profile: 12th – 19th August 2008.*

The key difference between the polar cells and the two other atmospheric cells present in the Earth's atmosphere, is that in summer the high latitude polar regions experience months of continuous daylight. The effect of continuous daylight is that any atmospheric convective activity, that results in vertical overturning in the Polar cell, returns air back onto a lit surface. This return of air onto the illuminated surface effectively short circuits the surface energy partition process, and delivers an energy flux boost directly back to the lit summer Polar cell environment.

By contrast, during their respective winter season, each Polar cell experiences months of continuous darkness and there is no direct input of radiant solar energy. Consequently, all of the energy flux experienced by the cells throughout the months of continuous darkness is a direct result of advected air transported into the polar environment from the abutting Ferrel cell.

In order to address the dichotomy of continuous summer illumination and continuous winter darkness, the design of the adiabatic model of the Polar cell was altered to incorporate the convective feedback process of summer, and also the advected process of winter into two separate modelling streams. For the purposes of this analysis, and as merely a scoping proposal, the average Polar cell summer temperature is assumed to be plus 5°C, and the average winter temperature is assumed to be minus 45°C. These two separate seasonal values combine to create the required average annual temperature for the Polar cell of minus 20°C (Table 11).

Table 11. *The inverse modelling process used to determine the seasonally separated dual power intensity flux partition ratios for the Earth's Polar cells.*

Cycle Number	Polar Incoming Captured Radiation	Heating the Summer Polar Cell	Summer Polar Thermal Radiant Loss to Space	Summer Polar Cell Return to Surface	Winter Air Advected from Ferrel Cell	Retained in the Winter Polar Cell	Winter Polar Cell Radiant Loss to Space	Winter Polar Cell Cold Air Returned to Ferrel Cell
	Polar Partition Ratio: Target Summer Temperature 278 Kelvin (5°C)		32.1957%	67.8043%	Polar Partition Ratio: Target Winter Temperature 228 Kelvin (- 455°C))		64.0791%	35.9209%
0	160.81				273.33			0
1	160.8064999	160.8064999	51.7728363	109.0336636	273.3325458	273.3325458	175.1490034	98.1835424
2	160.8064999	269.8401635	86.8770269	182.9631366	273.3325458	371.5160883	238.0641223	133.4519660
3	160.8064999	343.7696366	110.6791650	233.0904716	273.3325458	406.7845119	260.6638065	146.1207053
4	160.8064999	393.8969716	126.8180294	267.0789421	273.3325458	419.4532512	268.7818192	150.6714320
696	160.8064999	499.4652071	160.8064999	338.6587071	273.3325458	426.5549856	273.3325458	153.2224397
697	160.8064999	499.4652071	160.8064999	338.6587071	273.3325458	426.5549856	273.3325458	153.2224397
698	160.8064999	499.4652071	160.8064999	338.6587071	273.3325458	426.5549856	273.3325458	153.2224397
699	160.8064999	499.4652071	160.8064999	338.6587071	273.3325458	426.5549856	273.3325458	153.2224397
700	160.8064999	499.4652071	160.8064999	338.6587071	273.3325458	426.5549856	273.3325458	153.2224397
Cycle Number	Proportionate Polar Insolation	Heating the Summer Polar Cell	Summer Polar Thermal Radiant Loss to Space	Summer Polar Cell Return to Surface	Winter Air Advected from Ferrel Cell	Retained in the Winter Polar Cell	Winter Polar Cell Radiant Loss to Space	Winter Polar Cell Cold Air Returned to Ferrel Cell
Infinity	160.81	499.47	160.81	338.66	273.33	426.55	273.33	153.22
S-B	5.67E-08	5.67E-08	5.67E-08	5.67E-08	5.67E-08	5.67E-08	5.67E-08	5.67E-08
Kelvin	230.8	306.4	230.8	278.0	263.5	294.5	263.5	228.0
Celsius	-42.2	33.4	-42.2	5.0	-9.5	21.5	-9.5	-45.0

Statistic	Mean Exit Temp	Mean Air Temp	Summer W/m2	Winter W/m2	Polar Average W/m2
Kelvin	247.13	253.00	499.465	338.659	419.062
Celsius	-43.61	-20.00			

Atmospheric Response	Thermal Enhancement (Kelvin)	Lapse rate K/Km	Tropopause Height (km)	
			Delta K	Km
Summer Polar Cell	75.6	8.8	75.6	8.6
Winter Polar Cell	31.0	8.8	66.5	7.5

We have now completed the individual modelling process for each of the Earth's three atmospheric cells [15, 16].

3. Discussion of the Modelling Results

The triple-cell parallel adiabatic model of Earth's climate is tuned to produce the expected value of the average annual atmospheric temperature of 288 Kelvin (15°C) using the previously established method of weighted area to determine the average annual temperature of the Earth (Table 3).

The results of the inverse modelling process demonstrate that to achieve a stable average air temperature and also an appropriate cell specific tropopause height, solar energy must be preferentially retained in the climate system by the air that is located over the lit portion of the Earth's surface (Table 12). Retention in favour of the air occurs because convection at the solar heated surface boundary is a turbulent process. In the presence of a gravity field solar heated air ascends by buoyancy displacement which removes it from contact with the ground. Because the solid ground surface of a planet is the primary low-frequency radiator, ascending air becomes decoupled from this surface and so retains its energy internally as it rises.

Thermal radiant exhaust of energy to space is the primary control on the ambient atmospheric temperature. Even under conditions of reduced atmospheric opacity, the ground surface radiator of the Earth continues to operate through the Infrared Window, first identified in 1928 as a critical component of atmospheric radiant energy transmission [7].

Under conditions of zero solar radiant loading, either at night or during the polar winter, the ground surface radiator continues to operate through the atmospheric infrared window. The nighttime is an environment of energy deficit, gasses are poor absorbers and emitters of radiant thermal energy, so they heat most effectively by contact with the sunlit warmed surface during the day, and cool most effectively by contact with the radiatively cooled ground surface by night.

The Antarctic winter temperature inversion profile (Figure 4) is a direct consequence of thermal equilibrium being established and maintained by the process of surface radiative cooling. This cooling is caused by direct radiative energy loss to space through the dry transparent atmosphere above the high elevation Antarctic icecap. The radiative process results in the development and maintenance of a surface air temperature inversion. Under these conditions the atmosphere delivers energy to the ground surface radiator, and consequently the energy partition ratio for the winter polar cell is heavily weighted in favour of radiant energy loss to space (Table 12).

Table 12. Results of the inverse modelling process used to establish power intensity flux partition ratios for the Earth's atmospheric cells.

Daily Atmospheric Cell	Lit side Partition Ratio		Lit side	Dark side Partition Ratio		Dark side
	Thermal Radiant Loss to Space	Thermal Export to Dark Side	Tropopause Height (km)	Thermal Radiant Loss to Space	Thermal Return to Lit side	Tropopause Height (km)
Hadley cell: Target Annual Temperature 300.9 Kelvin (27.9°C)	24.1541%	75.8459%	18.0	53.8273%	46.1727%	10.4
Ferrel cell: Target Annual Temperature 279.5 Kelvin (6.5°C)	21.6206%	78.3794%	13.0	54.2258%	45.7742%	6.7
Seasonal Atmospheric Cell	Summer Polar cell Thermal Radiant Loss to Space	Summer Polar cell Thermal Return to Surface	Tropopause Height (km)	Winter Polar Cell Thermal Radiant Loss to Space	Winter Polar Cell Cold Air Returned to Ferrel Cell	Tropopause Height (km)
Polar cell: Target Summer Temperature 278 Kelvin (5°C)	32.1957%	67.8043%	8.6			
Polar cell: Target Winter Temperature 228 Kelvin (-45°C)				64.0791%	35.9209%	7.5

3.1. Studying the Effects of Energy Flux Variations Within the Adiabatic DAET Model

In conducting the modelling analysis presented here the key question that must be addressed is this. What is the justification for using energy partition ratio as the basis for determining the average annual temperature of the Earth?

There are three fundamental physical parameters that underpin our DAET modelling process that relate directly to planetary climate, these are: -

1. Global Atmospheric Temperature.
2. Global Atmospheric Pressure.
3. Global Atmospheric Volume.

We have already demonstrated that if we know the areal weighting of the three atmospheric cells, their respective tropopause heights, their TOA temperatures and also respective lapse rates, then the global average temperature of the planetary atmosphere can be calculated. We also know that the average pressure of the atmosphere can be determined by measurement and is common across all three cells, so the remaining issue is the determination of the planetary atmospheric volume.

If we assume that the tropopause is a pressure related phenomenon, and that the 100 mb pressure marks the upper limit of the troposphere [17], then the question of applying Boyle's Law to the total planetary atmosphere potentially has merit and requires investigation. The key objection that the Boyle's Law relationship relates only to a confined volume of gas assumes that planetary atmospheres are completely unconfined. Clearly this is not strictly true, the total surface area of the Earth does not change, the total mass of the atmosphere, and therefore its pressure is also a fixed quantity.

So, in the presence of a gravity field that binds the atmosphere to the planet it follows that the volume change we observe associated with a change in tropospheric height for each atmospheric cell must be related to the temperature of that cell. Consequently, we can study the planetary atmosphere in total by treating it as a single gravity confined entity with measurable parameters of temperature, pressure and volume.

In order to test the relationship between atmospheric temperature, pressure and volume, a simple single hemisphere adiabatic model was created with an illumination intensity dilution divisor of integer 2. This model is assumed to have simple diabatic radiative cooling from the dark unlit hemisphere, and so a constant partition ratio of 50% radiant energy loss to space and 50% retention by the air was applied to this part of the model (Table 13).

Table 13. Testing the Whole Earth PVT Adiabatic Model.

Cycle Number	Incoming Captured Radiation	Heating the Lit side	Lit side Radiant Loss to Space	Lit side Thermal Export to Dark Side	Darkside Radiant Loss to Space	Darkside Thermal Return to Litside	Radiant Energy Exiting to Space
	Litside Variable Partition Ratio: Target Annual Temperature 288 Kelvin (15°C)	26.9553%	73.0447%	50.0000%	50.0000%		
0	472.267					0	
1	472.267	472.267	127.3008921	344.9661079	172.483054	172.483054	299.783946
2	472.267	644.750054	173.7941822	470.9558718	235.4779359	235.4779359	409.2721181
3	472.267	707.7449359	190.774629	516.9703069	258.4851535	258.4851535	449.2597824
4	472.267	730.7521535	196.9762889	533.7758646	266.8879323	266.8879323	463.8642212
2996	472.267	743.990	200.5444627	543.4450745	271.7225373	271.7225373	472.267
2997	472.267	743.9895373	200.5444627	543.4450745	271.7225373	271.7225373	472.267
2998	472.267	743.9895373	200.5444627	543.4450745	271.7225373	271.7225373	472.267
2999	472.267	743.9895373	200.5444627	543.4450745	271.7225373	271.7225373	472.267
3000	472.267	743.990	200.5444627	543.4450745	271.7225373	271.7225373	472.267
Cycle Number	Incoming Captured Radiation	Heating the Lit side	Lit side Radiant Loss to Space	Lit side Thermal Export to Dark Side	Darkside Radiant Loss to Space	Darkside Thermal Return to Litside	Radiant Energy Exiting to Space

Cycle Number	Incoming Captured Radiation	Heating the Lit side	Lit side Radiant Loss to Space	Lit side Thermal Export to Dark Side	Darkside Radiant Loss to Space	Darkside Thermal Return to Litside	Radiant Energy Exiting to Space
Infinity	472.27	743.99	200.54	543.45	271.72	271.72	472.27
S-B	5.67E-08	5.67E-08	5.67E-08	5.67E-08	5.67E-08	5.67E-08	5.67E-08
Kelvin	302.1	338.5	243.9	312.9	263.1	263.1	302.1
Celsius	29.1	65.5	-29.1	39.9	-9.9	-9.9	29.1
	Statistic	Mean Exit Temp	Mean Air Temp	Lit-side	Dark-side	Hadley Average	
	Kelvin	253.49	288.00	W/m^2	W/m^2	W/m^2	
	Celsius	-19.51	15.0	743.990	543.445	643.717	
	Atmospheric Response		Thermal Enhancement (Kelvin)	Lapse rate K/Km	Tropopause Height (km) Delta K	Km	
	Lit Hemisphere		36.4	6.0	94.6	15.8	
	Dark Hemisphere			6.0	49.8	8.3	

The energy flux within the model was then adjusted by varying the Bond albedo. For each increment of Albedo related radiant power intensity, the inverse modelling process was run to determine the lit surface energy partition ratio that restored the global atmospheric temperature back to a constant value of 15°C.

Because we are now adjusting the Bond albedo, the power intensity flux in our simple model varies from a maximum case of 680.5 W/m^2 [1361/2*(1-0.0)] for a totally absorptive Earth (albedo=0.0), down to a lower limit of 272.2 W/m^2, [1361/2*(1-0.60)] for a bright reflective Earth (albedo=0.60). The power intensity flux lower limit of 272.2 W/m^2 occurs because below this value it is impossible for the model Earth to maintain an average annual temperature of 15°C if its albedo becomes any brighter.
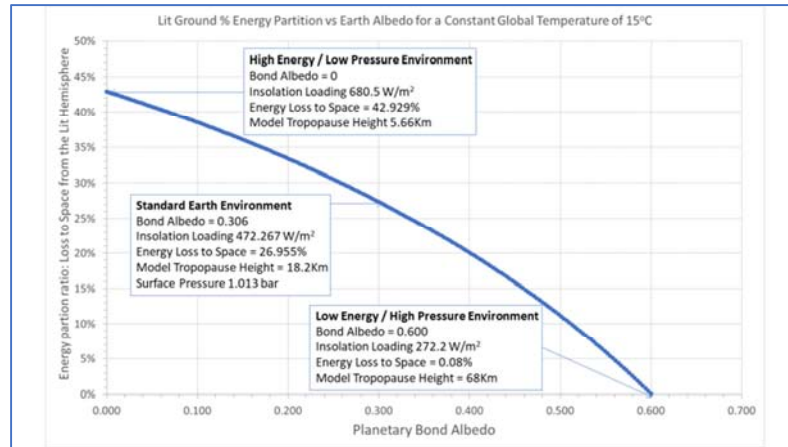
The results of these tests are shown in Figure 5.

Figure 5. The Variation of Energy Partition Ratio with Power Intensity Influx for a Single Lit Hemisphere Adiabatic Model.

Using data from the American Vacuum Society (AVS) the temperature and pressure profiles for the average atmosphere are shown in Figures 6 and 7 [18]. These data show that for a standard Earth atmosphere and a tropopause defined as occurring at a pressure of 100 mbar (Figure 6) then the average elevation of this pressure is at a height of 16 km (Figure 7).
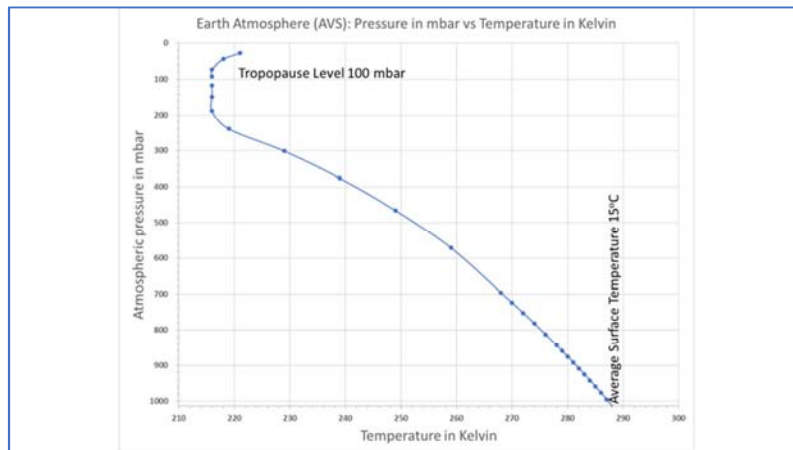

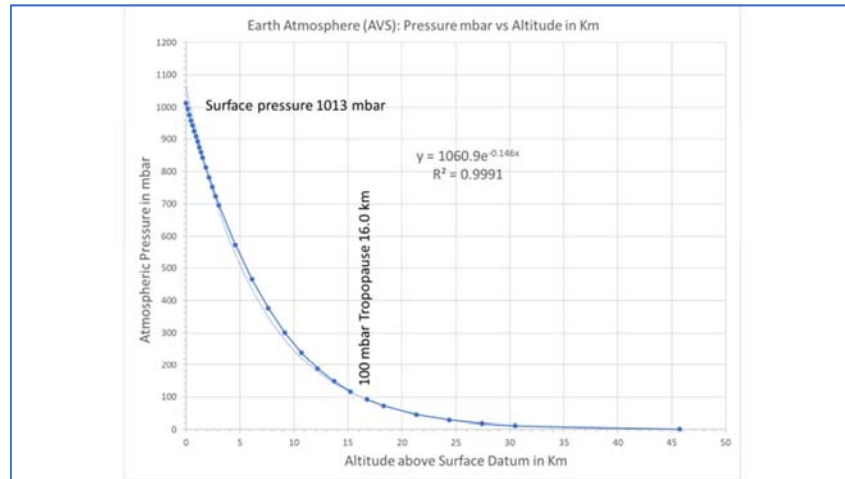*Figure 6. Earth's Average Atmosphere Temperature Profile (AVS data).*

Figure 7. Earth's Average Atmosphere Pressure Profile (AVS data).

Starting with a biased surface datum of minus 50 km, the calculated pressure versus height relationship for the Earth's standard atmosphere (Figure 7) was extended downwards to create a model high pressure atmosphere using an exponential pressure altitude equation (Km versus mbars):-

Equation 2: Pressure=1060.9*EXP (-0.146*C2) mbar

Where C2 is the Datumed Biased Altitude in kilometres.

Equation 2 is constructed to create the standard atmospheric pressure of 1013 mbar at the reference zero altitude of the Earth's surface under current atmospheric conditions. For Equation 2 negative altitudes relate to higher than ambient surface pressure, while positive altitudes relate to lower than ambient pressure. The calculated pressures range from a high pressure state for a model atmosphere thickness of 68 km (equation biased altitude of minus 50 km), down to a low

pressure state for a model atmosphere thickness of 5.66 km (equation biased altitude of plus 13 km) (Figure 8).

Using a model specific wet adiabatic lapse rate of 3.8 K/km for the lit side of the single cell model, the atmosphere "thickness" records a low of 5.66 km for the high solar energy input case, with a commensurate balancing high radiant energy loss to space. The maximum value of 68 km of atmospheric thickness is achieved for the low solar energy input case, and commensurate balancing low radiant energy loss to space (Figure 8). There is therefore a clear relationship between solar energy input and immediate energy shedding to space by the lit surface. This energy shedding is required to maintain the constant modelled average global temperature of 15°C, and is a pressure dependent effect (Figure 8).
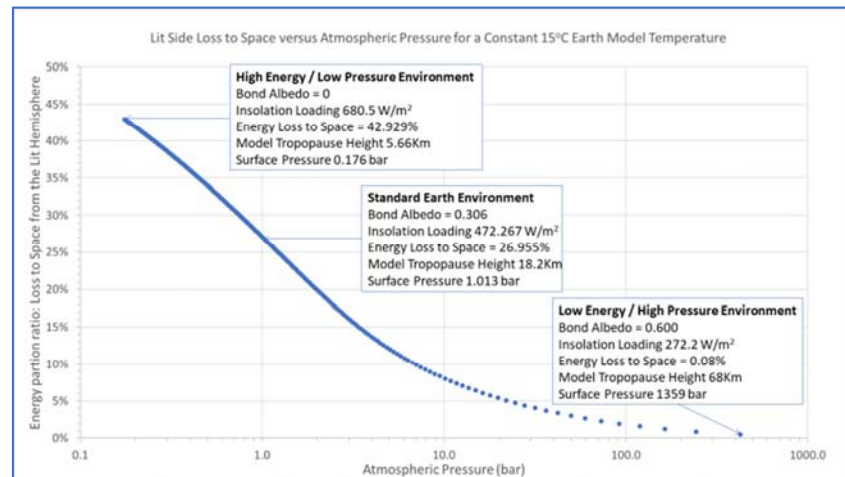

Figure 8. Lit Ground % Energy Partition vs Surface Atmospheric Pressure for a Constant Earth 15°C.

In Figure 8 we see the effective pressure dependent limits under which an Earth with an average planetary temperature of 15°C can exist for a given range of radiant energy loadings at its current orbital distance from the Sun. With the high albedo, (low energy capture) thick atmosphere end-member of the model we are effectively simulating a high pressure, low temperature version of the atmosphere of Venus.

3.2. The CERES Image of the Earth's Radiant Emission to Space

Each of the three atmospheric cells that constitute the circulation system of the Earth's atmosphere has a distinct set of meteorological parameters of areal extent, average insolation power intensity flux, average annual temperature

and adiabatic lapse rate. The following image (Figure 9) shows the Earth's outgoing long-wave radiation recorded by the CERES (Clouds and the Earth's Radiant Energy System) Instrument onboard the NASA Aqua Satellite [19].
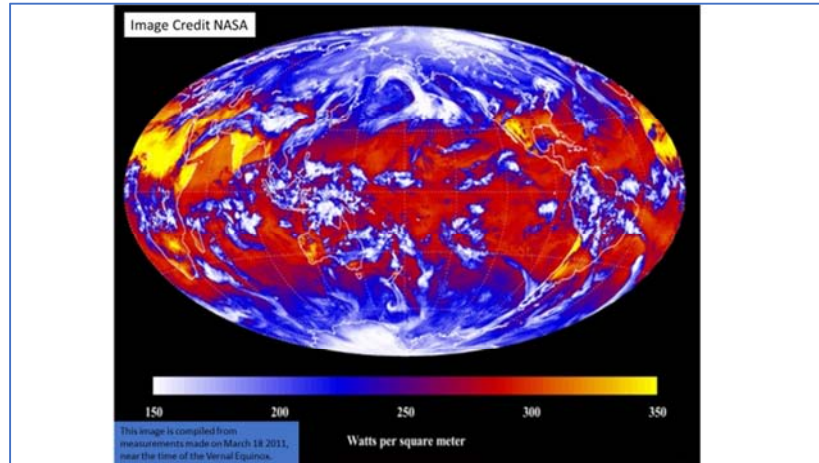

Figure 9. The Earth's outgoing long-wave radiation recorded by the CERES (Clouds and the Earth's Radiant Energy System) Instrument onboard the NASA Aqua Satellite [19, 20].

The colour table legend records the energy flux of the outgoing thermal radiation. This flux ranges from a minimum value of 150 W/m^2 displayed as white, to a maximum flux of 350 W/m^2, displayed as yellow. Using the Stefan-Boltzmann law of radiative emission these energy flux values can be converted to emission temperatures using the following equation: -

Equation 3: T=$(j*/\sigma)^{0.25}$

Where T is the thermodynamic temperature in Kelvin.

$j*$ is the black body radiant emittance in Watts per square metre.

σ is the Stefan-Boltzmann constant of proportionality.

(Sigma has a value of $5.670373 * 10^{-8}$ W m^{-2} K^{-4})

Using equation 3 we can determine that the emission temperatures recorded by the CERES instrument range from a minimum value of 226.8 Kelvin (-46.2°C) for the 150 W/m^2 low-end flux, to a maximum value of 280.3 Kelvin (7.3°C) for the 350 W/m^2 high-end flux.

3.3. Calibrating the CERES Image

The CERES image (Figure 9) is a single snapshot of the Earth's thermal radiant emission to space. This image contains a significant amount of information, however to understand this in its global context we must first calibrate the image against known measurements of the major components of the Earth's atmospheric system.

Visual inspection of the CERES image (Figure 9) shows the presence of cloud tops associated with the convective storms of the equatorial intertropical convergence zone (ITCZ) or doldrums. These storms are radiating at 150 W/m^2 and have an emission temperature of 227 Kelvin (-46.2°C). In order to determine the elevation of this emission, we need to use atmospheric parameters for the Hadley, Ferrel and Polar cells established in Section 2.3. (Table 2), which are:

1. The height of the tropopause.
2. The temperature of the tropopause.
3. The environmental lapse rate for each atmospheric cell.

Using the values established in Table 2 we can determine the top down temperature profile for each of the three atmospheric cells.

3.3.1. Calibrating the Hadley cell

The calculations for the Hadley cell show that to maintain a 17 km tropopause with a temperature of 190 Kelvin (-83°C) and a lapse rate of 6.5 K/km, then the average surface temperature of the tropical zone must be 301 Kelvin (27.9°C) (Table 14).

Table 14. Hadley Cell - CERES Image Emissions Calibration.

Energy Flux W/m^2	Kelvin	Celsius	Hadley Cell Profile Km	Radiant Depth Km	Hadley Cell Measurements
465	301	27.9	0.00		Average Tropical Surface Temperature
426	294	21.4	1.00		
389	288	14.9	2.00		
350	280	7.3	3.16	13.84	Maximum observed radiant emission depth of the Hadley cell seen from space
325	275	2.1	3.96	13.04	
309	272	-1.4	4.50	12.50	Tibetan Plateau 4500m
300	270	-3.3	4.80	12.20	
275	264	-9.1	5.69	11.31	
270	263	-10.4	5.89	11.11	Height of Kilimanjaro 5892m
250	258	-15.3	6.64	10.36	Midpoint observed radiant emission depth of the Hadley Cell seen from space
225	251	-22.0	7.68	9.32	

Energy Flux W/m²	Kelvin	Celsius	Hadley Cell Profile Km	Radiant Depth Km	Hadley Cell Measurements
200	244	-29.3	8.80	8.20	Height of Mount Everest 8850m
175	236	-37.3	10.03	6.97	
150	227	-46.2	11.40	5.60	Maximum supercooled liquid water atmosphere elevation in the Hadley cell
140	223	-50.1	12.00	5.00	
124	216	-56.6	13.00	4.00	
110	210	-63.1	14.00	3.00	
97	203	-69.6	15.00	2.00	
85	197	-76.1	16.00	1.00	
74	190	-82.6	17.00	0.00	Hadley Cell Tropopause Height

Converting this average surface temperature of ~28°C into a radiant energy emission flux, by using the Stefan-Boltzmann equation, we can establish that the tropical surface energy flux is 465 W/m². This value is 115 W/m² higher than the maximum observed flux of 350 W/m² in the Ceres image (Figure 9), and so we have established that this image does not record direct sea level surface radiant emission. Rather, with this image we are observing the atmospheric temperatures at elevations of 3,160 m (10,370 ft) and above. Consequently, all high elevation land surfaces in the latitude zone of 30°S to 30°N, such as the Tibetan plateau

at 4,500m (14,750 ft), will be capable of directly emitting thermal radiant energy to space through the overlying atmosphere.

3.3.2. Calibrating the Ferrel cell

The calculations for the Ferrel cell show that to maintain a 13 km tropopause with a temperature of 195 Kelvin (-78°C) and a lapse rate of 6.5 K/km, then the average annual surface temperature of the temperate zone will be 280 Kelvin (6.5°C) (Table 15).

***Table 15.** Ferrel Cell - CERES Image Emissions Calibration.*

Energy Flux W/m²	Kelvin	Celsius	Ferrel Cell Profile Km	Radiant Depth Km	Ferrel Cell Measurements
346	280	6.5	0.00		Average Temperate Surface Temperature
325	275	2.1	0.67		
300	270	-3.3	1.51	11.49	Maximum observed radiant emission depth of the Ferrel cell seen from space
275	264	-9.1	2.40	10.60	
250	258	-15.3	3.36	9.64	
225	251	-22.0	4.39	8.61	
200	244	-29.3	5.51	7.49	
190	241	-32.5	6.00	7.00	Height of Denali (Alaska) 6190m
175	236	-37.3	6.74	6.26	
150	227	-46.2	8.11	4.89	Maximum supercooled liquid water elevation in the Ferrel cell
135	221	-52.0	9.00	4.00	
120	215	-58.5	10.00	3.00	
106	208	-65.0	11.00	2.00	
93	202	-71.5	12.00	1.00	
82	195	-78.0	13.00	0.00	Ferrel Cell Tropopause Height

Converting this average surface temperature of 6.5°C into a radiant energy emission flux, by using the Stefan-Boltzmann equation, we can now establish that the temperate zone surface energy flux is 346 W/m². This value is 46 W/m² higher than the maximum observed flux in the CERES image of 300 W/m² for the temperate zone as seen from space (Figure 9). Once again, although this image does not record direct sea level surface radiant emission, all land surfaces with an elevation above 1,500 m (4,920 ft) will be capable of directly emitting thermal radiant energy to space through the

overlying atmosphere.

3.3.3. Calibrating the Polar cell

The calculations for the Polar cell show that to maintain a 9 km tropopause with a temperature of 194.5 Kelvin (-78.5°C) and a lapse rate of 6.5 K/km, then the average annual surface temperature of the polar zone will be 253 Kelvin (-20°C) (Table 16).

***Table 16.** Polar Cell - CERES Image Emissions Calibration.*

Energy Flux W/m²	Kelvin	Celsius	Polar Cell Profile Km	Radiant Depth Km	Polar Cell Measurements
232	253	-20.0	0.00		Average Polar Surface Temperature
225	251	-22.0	0.31	8.69	Maximum observed radiant emission depth of the Polar cell seen from space
200	244	-29.3	1.43	7.57	
175	236	-37.3	2.66	6.34	
169	234	-39.5	3.00	6.00	Elevation of North Dome, Greenland 3000m
150	227	-46.2	4.03	4.97	Maximum supercooled liquid water elevation in the Polar cell

Energy Flux W/m²	Kelvin	Celsius	Polar Cell Profile Km	Radiant Depth Km	Polar Cell Measurements
149	226	-46.6	4.09	4.91	Elevation of Dome Argus, Antarctica 4093m
134	221	-52.5	5.00	4.00	
119	214	-59.0	6.00	3.00	
105	208	-65.5	7.00	2.00	
93	201	-72.0	8.00	1.00	
81	194.5	-78.5	9.00	0.00	Polar Cell Tropopause Height

Converting this average surface temperature of -20°C into a radiant energy emission flux, by using the Stefan-Boltzmann equation, we can now establish that the polar zone surface energy flux is 232 W/m². This value is just 7 W/m² higher than the maximum observed flux in the CERES image of 225 W/m² for the region of the Southern Ocean, south of the Antarctic circle. This calculation demonstrates that all parts of the polar regions above 310 m (1,020 ft) elevation, and in particular the high elevation ice domes, will be capable of directly emitting thermal radiant energy to space through the overlying atmosphere.

4. Conclusions and Observations

1. By creating a dual surface climate model, with one day lit surface of energy surplus and a second dark night surface of energy deficit, we can apply two separate energy partition ratios to these two distinct environments, and study the impacts of these ratios on energy retention and distribution within the DAET climate model.
2. By assuming that the daytime environment on Earth is dominated by adiabatic convection and has an energy partition ratio weighted in favour of the air, we can account for the process of atmospheric uplift and energy retention by the air.
3. By assuming that the night-time environment on Earth is dominated by radiative cooling, and has an energy partition ratio weighted in favour of radiant loss to space, we can account for the standard nighttime air temperature profile, and the development of surface temperature inversions in air.
4. By applying a process of inverse modelling, we can establish the values of the energy partition ratio for the Earth's lit daytime and dark night-time environments. It is this daytime energy retention in favour of the air that creates the climatic thermal enhancement observed on Earth.
5. By using the appropriate adiabatic lapse rate for each cell, our inverse modelling process can be tuned to replicate the expected tropopause height for the Earth's tropical Hadley Cell of energy surplus, that of the temperate Ferrel cell, and also the height for the Earth's Polar Cell of energy deficit.
6. By constructing a simple single lit hemisphere adiabatic model, the range of energy partition ratios required to maintain a constant whole Earth temperature under various solar radiation loadings can be explored. Using an extrapolated pressure altitude equation, the relationship between the energy partition ratio for the lit surface of energy collection and confining atmospheric pressure can be established.
7. Convection efficiency is a pressure related phenomenon. High pressure gaseous environments are more efficient at removing energy from a solar heated surface in the presence of a confining gravity field.
8. Our modelling studies suggest that the opacity of the atmosphere fundamentally controls the height of the radiant emission surface that vents energy to space (as *per* [17]). However, there is no requirement for opacity to be an atmospheric energy amplifier via radiative feed-back *contra* [8].

In our analysis of the CERES image (Figure 9) we are looking at climate from a geological perspective. Our motivation for this approach was to try and determine if high elevation solid surfaces, such as the Tibetan Plateau, are "thermally visible" from space, and if the contrast in global land surface elevation between the Cretaceous and the Tertiary Periods can provide a physical explanation for the long-term planetary cooling of the Earth over the last 65 million years.

This analysis is based on the following points: -
1. All planets shed energy to space via thermal radiation.
2. Flexure of solid materials is the fundamental process that interlinks vibrating matter with thermal radiation. The coincidence of the lowest thermal radiant temperature of -46.2°C in the CERES image with the lowest observed temperature of super-cooled water suggests that there is a relationship between planetary Bond albedo and atmospheric thickness (Tables 14, 15, 16). Albedo therefore could be an emergent consequence rather than a cause of planetary climate.
3. Solid surfaces (either rock or ice) held at high elevation are efficient radiators precisely because they are composed of flexible materials.
4. Icecaps can melt, therefore the ice age high elevation solid ice surfaces of Canada and Scandinavia can rapidly disappear with major implications for surface radiation loss, whereas the Tibetan plateau with an elevation of 4,500m remains as a long-term geological high elevation radiant leak point (Table 14).
5. The apparent coincidence between the maximum elevation of the Antarctic Icecap at Dome Argus (4093m) and the maximum elevation at which super-cooled liquid water can exist in the atmosphere of the Polar cell (4030m) requires further study (Table 16). A possible explanation is that once the ice surface rises above the point where it is no longer possible to have

supercooled liquid water droplets in the atmosphere, then there is no further possibility for latent heat of crystallisation to be released. Therefore, there is no energy left in the meteorological system to power moist convection, and so vertical ice accumulation stops.

6. On Earth the rapid daily rotation limits the latitudinal reach of the Hadley cell [21, 22], it creates forced descent of upper atmospheric air in the mid-latitudes and directly accounts for the existence of the Ferrel cell. The Ferrel cell is a mechanical cell that acts as a cog between the tropical thermal Hadley cell of solar heating and energy surplus, and the thermal Polar cell of surface radiant cooling and energy deficit.

7. The impact of the forced descent of Hadley cell air in the mid-latitudes can clearly be seen in the CERES image (Figure 9). This descent creates a zone of high surface pressure and reduced moist convection that allows for significant planetary thermal loss to space over continental land areas, such as the Sahara Desert of North Africa. Over the adjacent mid-Atlantic and southern Indian Oceans, the same latitudinal zone of forced air descent allows for clear skies that lead to solar energy capture and retention by the marine waters below.

Our fundamental criticisms of the standard radiative climate model currently used by climate science are as follows: -

First, all materials heat and cool diabatically (laminar exchange of energy through the surface interface), solids do not significantly change their position when they are heated. Gaseous atmospheres not only heat and cool diabatically, but in addition air also heats *adiabatically*, which is a turbulent motion process of energy acquisition, and is a critical part of daytime surface heating.

Second, it is physically impossible to lose potential energy by radiant thermal emission. Atmospheric adiabatic energy transport is a meteorological process that delivers energy, without any transport loss, to a distant surface that is itself undergoing diabatic cooling by radiant thermal emission to space.

We have designed our climate model to retain the critical dual surface element of a lit globe, namely night and day. The standard climate model is a single surface model that does not include adiabatic energy transfer, because diabatic thermal equilibrium is assumed at all times (both night and day). When in our model we apply the missing element of adiabatic energy transfer from the lit side, by using distinct and separate energy partition ratios for night and day, then the requirement for back radiation greenhouse gas heating is no longer necessary.

We are able to quantify the degree of adiabatic lit surface energy partition in favour of the air by using the process of inverse modelling, a standard geoscience mathematical technique. The issue of atmospheric opacity then becomes a passive process, and the purported atmospheric action of greenhouse heating by back-radiation can be discounted. We believe that our modelling work presented here should lead to a fundamental reassessment of the atmospheric processes relating to energy partition, retention and flow within the Earth's climate system.

References

[1] Rosenberg, M. 2020 "Temperate, Torrid, and Frigid Zones." ThoughtCo, Feb. 11, 2020 https://www.thoughtco.com/temperate-torrid-and-frigid-zones-1435361.

[2] Persson, A. O., 2006. Hadley's principle: understanding and misunderstanding the trade winds. *History of meteorology*, *3*, pp. 17-42.

[3] Qian, W., Wu, K. and Liang, H., 2016. Arctic and Antarctic cells in the troposphere. *Theoretical and Applied Climatology*, *125* (1-2), pp. 1-12.

[4] Wang, W. L., Wang, Y. and WU, R. S., 2005. A new view on the Ferrel cell. *Chinese Journal of Geophysics*, *48* (3), pp. 539-545.

[5] Mulholland, P., Wilde, S. P. R., 2020. An Inverse Climate Modelling Study of the Planet Venus. *International Journal of Atmospheric and Oceanic Sciences*. Vol. 4, No. 1, 2020, pp. 20-35. doi: 10.11648/j.ijaos.20200401.13.

[6] Persson, A. O., 2005. The Coriolis Effect: Four centuries of conflict between common sense and mathematics, Part I: A history to 1885. *International Commission on the History of Meteorology 2,* 24pp.

[7] Simpson, G. C., 1928. Some Studies in Terrestrial Radiation. *Royal Meteorological Society (London) Memoir, Vol II. No. 16,* pp. 69-95.

[8] Kiehl, J. T and Trenberth, K. E., 1997. Earth's Annual Global Mean Energy Budget. *Bulletin of the American Meteorological Society, Vol. 78 (2).* pp. 197-208.

[9] Sagan, C. and Chyba, C., 1997. The Early Faint Sun Paradox: Organic Shielding of Ultraviolet-Labile *Greenhouse Gases. Science, 276 (5316),* pp. 1217–1221.

[10] Mulholland, P., Wilde, S. P. R., 2020. An Iterative Mathematical Climate Model of the Atmosphere of Titan. Journal of Water Resources and Ocean Science. Vol. 9, No. 1, 2020, pp. 15-28. doi: 10.11648/j.wros.20200901.13.

[11] Beal, A., 2011. The Surface Area of a Sphere Between Parallel Planes. Online Blog. http://www.usrsb.in/The-Surface-Area-of-a-Sphere-Between-Parallel-Planes.html.

[12] Williams, D. R., 2019. Earth Fact Sheet. NASA NSSDCA, Mail Code 690.1, NASA Goddard Space Flight Center, Greenbelt, MD 20771.

[13] Rubin, M. J., 1953. Seasonal variations of the Antarctic tropopause. Journal of Meteorology, 10 (2), pp. 127-134.

[14] Australian Antarctic Division 2008: Dome Argus http://www.antarctica.gov.au/living-and-working/stations/other-locations/dome-a.

[15] Mulholland, P., 2019a. Earth Adiabatic Parallel Model 20Jun19 Excel Workbook. Research Gate Project: Dynamic-Atmosphere Energy-Transport Climate Model.

[16] Mulholland, P., 2019b. Earth Adiabatic PVT Model 20Jun19 Excel Workbook. Research Gate Project: Dynamic-Atmosphere Energy-Transport Climate Model.

[17] Robinson, T. D. and Catling, D. C., 2014. Common 0.1 bar tropopause in thick atmospheres set by pressure-dependent infrared transparency. *Nature Geoscience, 7 (1),* pp. 12-15.

[18] American Vacuum Society (AVS) Atmospheric Pressure at Different Altitudes https://www.avs.org/AVS/files/c7/c7edaedb-95b2-438f-adfb-36de54f87b9e.pdf.

[19] Wanucha, G. 2014. The missing piece of the climate puzzle.

MIT News http://news.mit.edu/2014/global-warming-increased-solar-radiation-1110.

[20] Damadeo, K. and Hanson, H. 2017. CERES Clouds and the Earth's Radiant Energy System. NASA 9pp.

[21] Hunt, B. G., 1979. The Influence of the Earth's Rotation Rate on the General Circulation of the Atmosphere. Journal of the Atmospheric Sciences, Vol. 36 (8), 1392-1408.

[22] Del Genio, A. D. and Suozzo, R. J., 1987. A Comparative Study of Rapidly and Slowly Rotating Dynamical Regimes in a Terrestrial General Circulation Model. Journal of the Atmospheric Sciences, Vol. 44 (6), 973-986.